Title: **NorthWest Africa 6232: Visible-near infrared reflectance spectra variability of an olivine diogenite**

Authors: Carli Cristian[1], Pratesi Giovanni[2,3], Moggi-Cecchi Vanni[3], Zambon Francesca[1], Capaccioni Fabrizio[1], Santoro Simone[2]
1 – IAPS-INAF, via fosso del cavaliere 100, 00133, Rome (Italy)
2 – Department of Earth Science, University of Florence, via La Pira 4, 50121, Florence, Italy
3 – Natural History Museum of University of Florence, via La Pira 4, 50121, Florence, Italy

**Abstract**
Visible and near-infrared (VNIR) reflectance is an important spectroscopic technique to identify minerals, and their associations, on planetary bodies surface. Howardite, eucrite and diogenite (HED) are igneous-like meteorites with spectral properties suitable for 4Vesta and Vestoids.
Pyroxene and olivine are the two major mafic minerals present in HED which can be identified with VNIR reflectance measurements. Understanding the compositional variability of those phases and their mixtures, can be useful to better understand the evolution of 4Vesta crust. To reach this aim, laboratory activity on different diogenite or eucrite are important to explore their spectral variability and so our capability to retrieve compositional information.
Here we report the VNIR reflectance spectral analysis of an harzburgitic olivine diogenite, NorthWest Africa 6232 (probably paired with NorthWest Africa 5480), containing variable amount of olivine as small grains or aggregates. We evidence how the olivine-diogenite spectra parameters (e.g. position) are in accordance between slab and powders. The olivine-diogenite band position shifts from synthetic orthopyroxene in accordance with the presence of olivine and chromite. In particular, the presence of a large olivine clast permits to evidence a linear variation of the band position from synthetic orthopyroxene and olivine, but underestimating the presence of olivine in the olivine-diogenite spot.

## 1. Introduction

Diogenites (D) are achondrites meteorites, like orthopyroxenite and harzburgite, generally associated to a basaltic magmatism linked to the earliest stage of asteroidal melting on a differentiated parent body. They are petrogenetically correlated to eucrite (E), which can be cumulitic or basaltic, and to howardite (H), that are brecciated samples composed by diogenite and eucrite fragments. This suite of meteorites, named HEDs, is considered to be associated to a basaltic magma system on asteroid 4Vesta, which is considered their parent body (e.g. Feierberg and Drake 1980, McSween et al. 2013).

Diogenites are often characterized by orthopyroxene (opx), relatively Mg-rich (En84-66), associated with olivine (ol), spinel (e.g. chromite), sulfides and metals, and minor plagioclase, clinopyroxene, silica phase or rare phosphates (see summary in Mittlefheldt et al 1998, Grady et al. 2014). Depending on the modal composition, diogenites can be distinguished in dunitic (≥90% ol), harzburgitic (ol + opx) and orthopyroxenitic (≥90% opx), respectively (Beck and McSween 2010).

The presence of ol has been considered an important marker for the 4Vesta evolution (Pieters et al. 2005). Ol has been along searched within diogenitic terrains, but none of these regions (e.g. Rheasilvia) seems to have spectral evidence of this mineral phases (Ammannito et al. 2013a). Conversely it is discussed the presence of Ol in relative high abundance in northern regions, like Bellicia and Aruntia craters (Ammannito et al. 2013b) associated with

howardite-like lithologies enriched in eucrite (Zambon et al., 2014; 2016). Other regions with lower ol amount have been discussed by Ruesch et al. (2014), Palomba et al. (2015), Poulet et al. (2015) and Zambon et al. (2016). Several of these ol-bearing regions seems to be correlated with diogenitic material (Zambon et al. 2016).

The correlation between HED and 4Vesta is strongly suggested by VNIR reflectance spectroscopy. Several powdered portions of HED have been measured, as a bulk, showing reflectance spectra dominated by two crystal field absorptions around 1 and 2 μm (e.g. Duffard et al., 2005; Burbine et al., 2009; Beck and McSween, 2010). These absorptions are associated to pyroxene (px) (Burns 1993), the spectrally dominating phase in both diogenites and eucrites.

The compositional variation from diogenites to eucrites, due to both mineral phases and mineral chemistry, can be outlined also in VNIR reflectance. In fact, the crystal field absorptions due to transitional elements (i.e. Fe, Ti) are active in the VNIR, and so diagnostic to recognize silicates present on igneous material.

A shift from of the absorption positions low to high wavelength, for both 1 and 2 μm bands (band I and II, respectively) have been highlighted (e.g. Mittlefehldt et al 1998). This trend can be mainly identified with the increasing of iron and calcium in eucrite-px with respect to diogenite-px (Burbine et al. 2009, Beck et al. 2011). Anyway the presence of significant amount of other phases, e.g. plagioclase in eucrite and, in particular, of ol in diogenite (but also in some eucrites) could influence the reflectance spectra.

Recently, the presence of ol on 4Vesta for the first time indicated in Ammannito et al. (2013b) stimulated the discussion about the capability to retrieve the presence of ol in a mafic mixed material.

The major evidence attributed to the olivine was a clear asymmetry present at longer wavelengths with respect to the band center around 1μm (see Ammannito et al 2013b), similar to that singled out by generic ol-px mixtures. No ol absorption has been evidenced (Ammannito et al. 2013b; Poulet et al. 2015) from VIR data (onboard Dawn, e.g. De Sanctis et al. 2010), but studying spectral parameters (Ruesh et al. 2014; Thangjam et al 2014; Palomba et al. 2015) and modeling the spectra by radiative transfer (Poulet et al. 2015) or linear modeling (Zambon et al. 2016) variable abundance of ol has been retrieved on different site.

Anyway most of these methods have been tested considering mixtures of ol and px, where often ol was more forsteritic (Fo~86-90%) and px more enstatitic than in diogenite. Few work considered powders of HED with ol enriched samples or referred to them (e.g. Li and Milliken 2015; Beck et al. 2013).

Beck et al. (2013) working with a systematic ol (Fo90) and px (En76) powder mixtures highlighted a linear trend between the 1 and 2 μm Band Area Ratio (B.A.R) and the px%. Such trend was already evidenced by Cloutis et al (1986) for a Fo89-En86 set of ol-px mixtures, grinded at different sizes. Cloutis et al (1986) discussed also how this trend was not size dependent. Beck et al. (2013), studying some harzburgitic diogenite meteorites, demonstrated that the B.A.R was not so different from a orthopyroxentic diogenite, and compatible with relative low ol amount (<30%), although they emphasized the heterogenous distribution of ol within the same diogenite sample.

Moreover, a correlation between the band I position and the B.A.R parameter has been evidenced by Cloutis et al. (1986) and Gaffey et al. (1993), even if varying the mineral composition, mineral assemblages and grain size this trend can vary (Pieters et al. 2005).

Recently, Li and Milliken (2015) working with a radiative transfer model show a good fit some fine powder spectra of ol-bearing diogenite. The authors worked with retrieved optical constant from spectra of compositional reasonable endmembers with fine size. They reported a good accordance (within 5%) of olivine amount.

So studying opportune material as analogue mixtures or HED meteorites in details can contribute to better understand the ol spectral influence on px absorptions with suitable mineral chemistry; and consequently to investigate in higher detail the amount of olivine on Vesta terrains.

Spectrally investigating meteorites samples as powders implies that few sample can be studied. Moreover, powders homogenize the distribution of the mineral phases present in the sample (which can be highly variable) loosing information about sample heterogeneity (at least at the observing scale). In addition, looking for HED analogues, the difference in composition with respect to terrestrial rocks avoids or complicates to obtain systematic mineral mixtures with suitable Fo/Fa and En,Fs,Wo. Moreover the presence of plagioclase (in particular for eucrite) and other minor, but effective, constituent (like chromite, sulfides and metal) are not considered.

A different opportunity to enlarged the number of samples but in particular the spectral variability due to all the rock constituent on HED is to analyze spectral properties of representative slices (slab), well characterized from a petrographic and mineral chemistry point of view.

Slab spectra suffer the effects of petrographic characteristics and effect due to the optical coupling which can strongly influence the slope and absorption spectral contrast. However, bulk rock spectra can contribute to the spectral description of a natural rock suite, adding spectral information needed for the interpretation of remote sensing or in situ high-spatial resolution hyperspectral data.

Few works in the literature discuss the spectral variation between slab and powders from the same rocks, Harloff and Arnold (2000) and Pompilio et al (2007), evidence how spectral contrast and slope can vary, even if the dominating spectral features relate to crystal field are always evident. Carli et al. (2014) highlighted how in co-genitic mafic/pl-bearing rock powders and slabs permit to define the same lithological units from VNIR spectra. Moreover, different works emphasize how coarsening the particle or grain size do not strongly effect the band center of minerals (e.g. Craig et al., 2008; Serventi et al. 2013;2016). This appears true also for large sizes up to slabs (e.g. Carli et al., 2014; 2015) even if it has been evidenced how coarsening the sizes the most abundant minerals became more effective even if less absorbing (e.g. pl versus px, see Serventi et al., 2013, Carli et al. 2014). Conversely, the band depth varies with the size (e.g. Craig et al 2007; 2008) even if systematic trend can be always recognized for the different sizes with respect the mineral abundances or volumetric iron (Carli et al. 2014).

In this manuscript we described the spectral properties of an harzburgitic olivine-diogenite, NorthWest Africa 6232 (NWA6232) classified by A. Irving and S. Kuehner (see, Garvie 2012) and probably paired with NorthWest Africa 5480 (NWA 5480, comment submitted by A. Irving on Meteoritical Bulletin Database). We considered spectra of both powders and two slabs, for which we acquired several spectra with particular attention to few spots with ol or px dominated region. Besides, due to the presence of a coarse ol clast we discuss the implication for the retrieving of compositional information from harzburgitic diogenite considering spectral parameters unaffected by the size.

## 2. Methods and Analytical approach

### 2.1. Sample Preparation and characterization

Two slices of NWA6232 harzburgitic olivine diogenite, belonging to the Natural History Museum of the Università degli Studi di Firenze (cat. n. RI-3225), have been analyzed. Both slices (here labelled NWA6232_A and NWA6232_B) have been considered as slab samples for reflectance investigation. Additionally, from the second slice a thin section was obtained for petrographic and minerochemical analyses. Moreover, from a representative portion of the diogenite NWA6232_B we produced powders at different grain size.

Asperities left by the saw were not present on measured cut surface samples, so we do not treated slabs further and, therefore, the slab do not show a mirror-like surface.

To preserve the original meteorite composition in powdered samples, the rocks were first ground to prepare the <1.00 mm coarse grain size class. The coarse powders were then quartered and each fraction was ground under smaller grain size classes, <0.050, <0.075, <0.100, <0.125, <0.150, <0.180, <0.200, <0.250 mm.

Mineral assemblages and rock textures were first observed, on thin section, through a Zeiss Axioplan II optical microscope. Then, scanning electron microscope images and elemental maps were acquired, on both the first slab and the thin section, at the MEMA laboratories of the University of Firenze by means of a Zeiss EVO MA15 equipped with OXFORD INCA 250 microanalysis. In order to get the relative modal abundance of the main mineral, the elemental maps (Si, Al, Mg, Fe, Ca, Mn, Cr, S) were processed with the specific INCA software module. Finally the minero-chemical analyses of the main phases (namely olivine and pyroxene) were performed, at the microanalysis laboratory of the IGG-CNR by means of Electron Microprobe JEOL JXA-8600 equipped with four Wavelength Dispersive Spectrometers. The modal and mineral chemistry analyses are reported in Tables 1, 2.

### 2.2. Sample Reflectance Measurements

Bidirectional spectra of slabs and powders, at different grain sizes, were acquired using a Fieldspec Pro ® spectrophotometer mounted on a goniometer at S.LAB. laboratory, at "Institute for Space Astrophysics and Planetology", IAPS-INAF, Rome. The spectra were acquired with a spectral resolution of ∼3 nm in the VIS and ∼10–12 nm in the NIR, a spectral resolution of 1 nm, with i = 30° and e = 0°. The source used was a quartz tungsten halogen (QTH) lamp and the spot illuminated has a diameter of ca. 6 mm. The standard reference calibration was performed with a Spectralon optical standard (registered trademark of Labsphere, Inc.) both for slab and powder measurements.

Therefore each powder grain size class (<0.050, <0.075, <0.100, <0.125, <0.150, <0.180, <0.200, <0.250 mm) contains a range of grain dimensions beneath the upper limit to maintain the compositional homogeneity. The slab samples are considered as analogs of centimeter-size natural rock grains and compact multimineral aggregates in the regolith (Carli and Sgavetti 2011). Studying both powders and slabs spectra evidences how varies the influence of the optical coupling with respect to the mineral absorptions. This aspect is very important (see also Carli and Sgavetti 2011) to understand spectral information of multi-crystal grains, which can be present in a regolith. By the way we can investigate the spectral heterogeneity of samples at the scale of the illuminated spot.

Moreover, the first slice (NWA6232_A) contains an olivinic clast with dimension closer to 6mm, so we acquired spectra along a cross line starting from the adjacent diogenite

185 portion and finishing into this clast. This set of measurements were then used to
186 extrapolate areal abundance of olivine with respect the diogenite sample from a spectral
187 parameters analysis.
188

189 ### 2.3. Correlation between spectral parameters and composition

190 Absorptions related to the crystal field of HEDs have been deeply investigated, and they
191 are in general due to the presence of pyroxenes. Different parameters, in particular, band
192 center position (B.C.), band depth (B.D.) and the B.A.R are frequently applied to
193 correlate spectral properties with the different lithologies, i.e. eucrite, diogenite and
194 howardite. The same parameters can be also calculated in presence of different amount of
195 olivine and can give also indication of the different amount of pyroxene and olivine.
196 Knowing the mineral chemistry and the petrography of our samples allows to better
197 explain the properties of acquired spectra from both powder and slab. Furthermore, it can
198 permit a comparison of the olivine diogenite with the spectral properties of the rock
199 forming minerals with the appropriate composition analyzed in the literature (e.g.
200 pyroxenes from Klima et al. 2007; olivine from King and Ridley, 1987, Sunshine and
201 Pieters, 1998, Isaacson et al. 2014).
202 Therefore, in section 3.3 we correlate the B.C. to the mineral chemistry of px and ol, and
203 the two B.C.s each other. B.D.s and shoulder position (maximum between Band I and
204 Band II) have also take into account to evidence the spectral variability. In addition, we
205 correlate also the spectral parameters of a cross in-out to an olivine clast evidencing the
206 spectral changes respect to the ol amount into the illuminated spot. This has been done
207 considering both shift of B.C.I and B.A.R, and their variability with ol% into observed
208 spot. We will refer as ol-cross to the spectra acquired along this cross.
209 The ol clast % in the illuminated spot has been calculated considering the clast as circular
210 (as the spot), so we calculated the integrated area between the two circle, moving on the
211 clast into the light spot along the diameter.
212 All the spectral parameters have been calculated after continuum removed. The
213 continuum is considered as a wavelength's function line segments that join the
214 reflectance maxima in the spectrum (Clark and Roush 1984). The reflectance maxima are
215 chosen for each case depending on the single spectrum.
216

217 ## 3. Results

218 ### 3.1. NWA6232, petrography and mineralogy

219 NWA6232 has been classified by A. Irving and S. Kuehner (Garvie, 2012) as a diogenite
220 but few characteristics have been reported by these authors. It is probably paired with
221 NWA 5480, a pristine harzburgitic diogenite characterized by an highly deformed texture
222 explained by plastic deformation that occurred after crystallization at mantle pressures
223 (Tkalcec et al., 2013 ; Peslier et al., 2015 ) or as an impact-melt breccia from a target
224 composed of olivine and pyroxene-rich lithologies (Yamaguchi et al., 2015 ). Here we
225 have described macroscopically the two slices, then a thin section of a representative
226 portion of one slice (NWA6232_B) has been investigated in detail under optical
227 microscope.

The thin section shows an heterogeneous overall texture characterized by a cumulitic intergrowth of olivine and orthopyroxene dominated zones (Fig. 1). Olivine ranges in size from tens of μm to mm: smaller grains are poikilitically included in orthopyroxene, while the largest grains are aggregates of smaller grains with variable orientation, which often display rounded edges and are most anhedral (Fig. s1, supplementary online). Orthopyroxene grains are typically subhedral and range from hundreds of μm to mm in size. They are riddled with poikilitic olivine and do not show any alignment. Chromite occurs as subhedral grains, 100 μm wide and with resorbed margins or as blebs < 10 μm wide. Troilite grains, often <10 μm in size, are scattered throughout the thin section. The hand size slice (NWA6232_B) shows also a centimetric grey area characterized by a concentration of pyroxene, not present in the thin section. The other slice of the sample, NWA6232_A has been observed and analyzed by means of SEM. The cut surface displays an hetereogenous texture similar to the one observed in the thin section, although a cm-sized clast of olivine is clearly distinguishable. BSE-SEM images and compositional maps (Fig. s2 and s3) performed on the slice allowed to determine the following average modal abundances of the phases of the diogenite: orthopyroxene 72%, olivine 26%, troilite 1%, chromite 1% and rare Fe,Ni alloy (see Table 1). The olivine clast appears homogeneous, although several chromite grains (circa 3%) are scattered throughout the clast (Fig. s4).

### 3.2. VNIR reflectance data of NWA6232

Twenty spectra have been, here, acquired for each slab sample to cover the entire surface, a cross of thirteen spectra have been also acquired from outside to inside the ol-clast (see table 3). In addition we acquired spectra for each powder grain size.

Reflectance spectra (Fig. 2b,c,d,e) show clearly the two absorption bands diagnostic of pyroxene for all the powder's spectra and for slab's spectra, with the exception for spectra around the above described olivine clast in NWA6232_A (Fig. 2a, and green dashed circle in Fig. 1a). A small portion of NWA6232_B shows two deeper absorption, this area seems to be characterized by higher concentration of pyroxene. In this manuscript, for clarity, we named ol-diogenite the collected spectra scattered overall the sample, ol-clast the spectra acquired on the 6 mm clast, ol-rich the spectra where diogenite reflectance properties are influenced by ol, px-rich the spectrum that is characterized by the strongest band I and II absorption.

Spectra dominated by pyroxene absorptions show also two weak absorption at 0.505 and 0.547 μm, associated with spin-forbidden $Fe^{2+}$ absorption (e.g. Burns 1993; Klima et al. 2007). A third weak absorption around 0.428 μm is evident only for the higher reflectance slab spectra and powders spectra (Fig. 3). Spectra dominated by olivine absorption show weak bands at 0.458 and at 0.496 μm, which can be correlated with spin-forbidden in olivine, and a third absorption around 0.529 μm (Burns et al. 1993).

The absorption around 0.5 μm is of particular interest because ol and px spin-forbidden are almost overlapped around those wavelengths. In fact, powder spectra show an asymmetric absorption, as well as ol-diogenite slab spectra, whereas ol-rich spots show a doublet minima (e.g. dark green spectra in Fig. 3b). Px-rich and Ol-clast spectra instead show the two different expected absorptions. Moreover, the ol-clast spectra have a wide and relatively weak absorption towards 2 μm which is not expected in ol spectra, but it

can be due to a small contribute of px, in particular, chromite (Burns et al. 1993; Cloutis et al. 2014).

Here, we focus on the two stronger absorptions at 1 and 2 μm to discuss the spectral variability with respect to the two dominating mineral phases. To reach this aim, aside from the spectra acquired on powdered sample and on two slabs (Fig. 3), we systematically measured spectra from a cross out to in the ol clast, described above, which have a size closer to the illuminated spot (Fig. 4).

### 3.3. Compositional variation by VNIR analysis

In this section, we report the result from spectral parameters and we compare it with the mineral chemistry, modal composition and phases distribution.

The band center for powders and the two slices (without ol dominating spots) have been plotted as averaged values in Fig. 5a,b with respect to the ferrosilite content (Fs%) in pyroxene. The position of Band I (B.C.I) shows a very reduced shift between powder and the two slices with a small standard deviation. Differently, powder Band II (B.C.II) spectra shows a shift to slight higher wavelengths compare to the two slices' spectra, which show higher standard deviation, even though within one sigma.

We have also considered the B.C.I and II of three synthetic pyroxenes from Klima et al. (2007) with mineral chemistry close to those present in NWA6232. The samples are named 002, 003, 027, in their paper, with Fs% varying from 20-30% (Klima et al. 2007). The px's B.C.I are 10 nm lower than NWA6232's B.C.I. This can be correlated with the presence of widespread crystals of olivine spread out in the diogenite. B.C.II of px shows position closer to those of the averages of slices spectra, whereas also in this case powder's spectra show a slightly shift towards higher wavelength.

The diagram B.C.I vs B.C.II permit to describe the spectral variability of pyroxene from low-Ca to high-Ca (e.g. Cloutis and Gaffey 1991), and it has been used to plot HED spectra and differentiate between diogenite and eucrite (e.g. Moskovitz et al., 2010). The compositional variation from high-Mg and low-Ca px in diogenite towards Fe- and Ca-enriched px in eucrite reflects an almost linear variation of B.C.I and B.C.II.

In Fig. 5c we plotted the averages B.C.I vs B.C.II for two slices, the powders and the Klima's px, for all we report the error bars representative of the standard deviation. It's clear that each spectrum, despite a range of variations, in particular for B.C.II is compatible with low calcium pyroxene. Nevertheless, B.C.I is slightly shift to longer wavelength and powder spectra show both centers at slightly higher wavelengths. If we compare these positions with HED spectra from literature (see dark and light grey box for diogenite and eucrite, after Moskovitz et al., 2010), we can see a good correspondence between band centers and diogenite field for slabs' spectra, except for ol-dominated spectra. The powders B.C.s are still in diogenite field but shifted towards eucrite field.

In Fig. 5c, we plot also the B.C.I position for olivine with closer fayalite (Fa%) value (from King and Ridley 1987; Sunshine and Pieters, 1998; Isaacson et al., 2014). The green lines represent the band center position (solid, Sunshine and Pieters, 1998; dot, Isaacson et al., 2014) calculated by Modifed Gaussian Model, as Gaussian minimum position (Sunshine et al 1990), and dashed line is the band center calculated as the minimum after continuum removed by King and Ridley (1987). The ol-rich and -clast spectra show B.C. close to the expected value for an 29 Fa%. These spectra show also a second band around 2 μm, but shifted to higher values with respect to other diogenite

spectra, in this olivine dominated spot (ol-clast) the second band could probably be assigned to the presence of chromite (e.g. Cloutis et al. 2004) as reveal by SEM images.

Considering the composition of px in NWA6232 and the spectra of pxs with analogue composition from Klima et al. (2007), we can assigned the shoulder at longer wavelength for the Band II between 2.45 and 2.50 μm (e.g. continuum removed spectra in Fig. 4c). For this reason, we considered, for powder and slab spectra, the maximum for the continuum between this wavelength range, varying for each spectrum, depending from the spectral shape and slope. So we can be confident that the shift in band center, after continuum removed, should be attribute to local variation in mineral assemblages (Fig. 4c).

Fig. 6 shows the variation of 1) Band Depth (B.D.), 2) the Shoulder Position (B.S.) vs. B.C. for Band I and Band II and the 3) Band Area ratio (B.A.R.) for all the measured spectra of NWA6232_A and NWA6232_B.

Band I depth varies from 0.2 to 0.5 (Fig. 6a), except for the px-dominated area (B.D.I ~0.7, as well as, B.D.II; Fig. 6b), without any correlation with band position. B.D.I and II of powder spectra are higher than those for slab spectra, but their depth are smaller with respect px-rich spot. Spectra dominated by ol-clast have a B.D.I around 0.5-0.6, and for the ol-cross the band depth seems to be correlated with the center position.

B.D.II seems to have a weak correlation with the position, decreasing the depth the absorption moves from lower wavelength, where band II is dominated by pyroxene, to longer wavelength, where probably increase ol and opaque phases (e.g. chromite), as suggested by ol-cross data. In fact, we can see the presence of two cluster indicating px-dominated spectra (ol clast < 10%, see table 3) and ol-influenced spectra.

B.S. is not a direct indicator of absorption, but in mixing material can give useful indication as demonstrated also by Serventi et al. (2013).

B.S. slightly moves from 1.3 to 1.5 μm (Fig. 6c) with a weak linear correlation with respect to px dominated B.C.I, whereas ol-influenced spectra move to high values (1.7 μm). Ol-cross data evidence as moving from diogenite to the ol clast there is a quick shift to longer wavelength of the B.S. up to 1.7 μm. This wavelength is reached for 006-007 spectra, which show a 39-48% of ol-clast (see table 3). B.S. vs. B.C.II (Fig. 6d), differently, show essentially two populations, with high values for ol clast>50% (B.C. II > 2.0 μm) or region with B.C.II at ca. 1.9 and B.S. at ca. 1.4 μm.

In Fig. 6e the B.C.I is plotted vs. the B.A.R parameter for the spectra acquired in the cross-in to olivine clast, superimposed to the results from Gaffey et al. (1993) modified after Pieters et al. (2005). Gaffey et al. (1993) trend was obtained by Cloutis et al. (1986) for powders' mixture (at three grain sizes 38-53, 63-90, 90-125 μm) of olivine (Fs89) and pyroxene (En86) with different mineral chemistry respect to NWA6232. Cloutis et al (1986) evidence how no-size effect where present. However, considering a modified B.A.R, and considering different compositions of px and ol, the variation of spectral parameters from the general trend was evident for some of the few investigated cases.

The presence of an ol-clast with a dimension closer to the illuminated spot can be used for a more quantitatively evaluation of the olivine influence on reflectance spectra when present with variable abundance into diogenite. Fig.6e shows a similar general behavior with respect to the one evidenced by Gaffey et al. (1993), with differences which could be related to the different size and in particular to mineral association.

Moreover, we measured the B.A.R also for powder spectra of NWA6232 and their values are in good agreement with respect to the values for the ol-diogenite spectra of the ol-cross (spot 000, 001 and 002, table 3).

Then, we have calculated the ol clast abundance as the ol area % presents in our spot (see section 2.3) to evaluate the variation of those spectral parameters which can be attributed to compositional information, such as B.C.I and B.A.R. We did this for all the thirteen ol-cross spectra measured at different steps (see table 3).

In Fig. 7a,b B.C.I and B.A.R. are plotted vs. the area of olivine present in the spot. It results clear that the variation in B.C.I, already evidenced in Fig. 6, is correlated with the variation of the area of olivine clast into the spot, with an almost linear trend ($R^2$=0.981). The B.A.R., considered by Cloutis et al. (1986) to be a possibly indicator to discriminate px/(px+ol), shows, in Fig. 7b, a strong reduction from values >1 to 0.2 for only 30% of ol-clast (000 to 004 spectra). Increasing the ol abundance B.A.R shift towards 0.1 for 100% of olivine clast in the spot.

From Fig. 5 we have seen that the diogenite B.C.I is shifted to values higher than pyroxene composition, and this could be in accordance with the widespread presence of olivine grains (from tens of micron to mm) in NWA6232 (see section 3.1 and Fig. s1). To investigate the influence of olivine present into the diogenite we have considered the opx B.C.I from Klima et al. (2007). Then we have on one side hypothesized a variable abundance of olivine also in ol-diogenite spectra (Fig. 7c), and on the other side we have considered the averaged abundance (25%) we obtained from SEM images. Considering a possible B.C.I linear trend from synthetic pyroxene to ol-clast we have seen that the best fit required an ol abundance for NWA6232 ol-diogenite spectra of 8% ($R^2$=0.988), with a variation from 5 to 11% of ol with $R^2$>0.985. Olivine abundance retrieved from SEM elementary maps image analysis indicates a higher value of olivine, which is variable within the different images but always upper than 20%. So the B.C.I shift of circa 10 nm from opx to ol-diogenite spectra (where circa 25% of olivine is present) then the position shift with an almost linear trend to 1.068 μm when the olivine clast is completely into the spot (011-012 have the almost same B.C.I position).

This is reasonable considering that opx crystal field absorption is strongly than co-genetic ol (e.g. Serventi and Carli, 2017) and opx absorption at circa 1μm insists within the lower wavelength portion within the ol absorption.

## 4. Discussion and implications for olivine detection on parental bodies

NWA 6232 is an olivine diogenite, characterized by an average abundance of ol close to 25%, present in size from tens of μm to mm, with smaller grains that are poikilitically included in opx and largest ones that are aggregates of several crystals. In one of the two samples a clast of ol crystal aggregates has dimension of circa 6 mm in diameter.

So, considering a spot of the same size we can evidence how vary the spectral properties and in particular some spectral parameters with the olivine abundance. The ol-opx variability has been already discussed in some cases (e.g. Cloutis et al., 1986; Beck et al., 2013), working with mineral mixtures, in the past, but often with ol and opx composition different from those expected for HED. Few cases investigate powder of ol-bearing diogenites but with only low range of relative ol abundance, even if this variability can be high on the same sample in abundance as well as crystal size.

Therefore, to investigate a slab becomes an important tool for up-grading the spectral variability of our meteorites samples, working with the opportune mineral composition, and mineral association as expected for their parental bodies. Moreover, due to the expected sample heterogeneity, we can evidence systematic variation on spectral properties and particularly in some spectral parameters (e.g. band position), which are no or few affected by the crystal or grain sizes. In our case, it plays an important role the presence of two regions, ol-dominated and px-dominated. In particular we took care about the ol-dominated region where a clast with dimension similar to our observing spot is present.

In general we have observed that spectra of ol-diogenite, for both slab or powders, are characterized by the two absorption bands indicative of pyroxene (Fig. 2c,e). The spectral features vary slightly in the wavelength region between 1.0 and 1.5 μm in accordance with a variable amount of olivine into the different spots (Fig. 2b). Only ol dominated spectra show a 1 μm absorption clearly indicative of this mineral (Fig. 2a), even if the ol-cross spectra show how a systematic variation is present varying the areal abundance of olivine in the spectra (Fig. 4b). Spin forbidden absorption seems to be present (already evidenced for HED, or px and ol, in the literature, e.g. Burns 1993; Hiroi et al. 2001, Klima et al., 2007; Isaacson et al., 2014). They are different in position for ol and px (Fig. 3a,b), but one absorption is centered at circa 0.5 μm for both ol and px, and it seems like it varies with the ol/px ratio.

The primary absorptions are around 1 and 2 μm, their position permit to superimpose NWA6232 into the Diogenite field (Fig. 5c), with some difference between slabs and powders, with the last that show centers at slightly longer wavelength. The average value for the slab spectra is closer to the synthetic pyroxene B.C. with Fs 25%, even if B.C.I is always shifted of ~ +10nm. Ol-clast spectra still show a residual BII which could be related to few amount of pyroxene into the spot, but because it is shifted towards longer wavelength, we can suppose that chromite plays a role (Fig. 5c and see Fig. s4).

We have seen that the Band I can be considered a useful indicator for discussing the ol/px relative abundance, as already indicated in the literature (e.g. Cloutis et al., 1986). Being the depth influenced also by the grain size, we highlighted that band center is an important parameter for this goal. In fact, comparing the B.C. with B.A.R (as in Pieters et al., 2005), we can see that our spectra closely follow the general trend, considering the difference in ol-px mineral chemistry and size effect. Ol dominated spot have also chromite grains within ol-clast, and ol-diogenite spectra are characterize by an averaged 25% of olivine widespread in the sample, so it is not a single opx endmember. Moreover, comparing the shift of the B.C.I varying the areal abundance of the ol clast, into the measured spot, we can see a linear trend (Fig. 7a); whereas the B.A.R reaches values very closed to the 100% of ol (Fig. 7b), already for 30% of ol-clast. Then, considering the opx endmember position (Fig. 7c) we can see that the ol abundance expected for the ol-diogenite spectra, considering the best linear fit, should be 8%, with a range 5-11% with very high $R^2$.

Anyway, analyzing our samples with SEM images (X-ray elementary maps) we have calculated a range of widespread ol grain into NWA 6232 between 20-35%. This indicates that increasing ol into our spot, the opx absorption strongly dominate the spectral parameter until 25-30% of olivine then band center start to follow a linear shift increasing the ol.

B.A.R, as well as the position of the B.S. between Band I and II, seem to be useful indicator of ol presence since they shift to values closer to those for the ol-clast spectra for ~ 50% of olivine (30% of ol clast, see fig. 6c and 7b).

These results can be considered a first test to evidence the spectral variability of an olivine diogenite as well as the ol/opx ratio with composition compatible for the diogenite. Therefore, them seem to evidence how persisting into slab analysis of HED, as well as other meteorites, e.g. associated to asteroids V and S, could contribute to better define spectral indicator for studying the composition of those bodies. In fact, often we referee to terrestrial analogues which have different mineral chemistry, as well as mineral assemblages, with respect to the composition of those meteorites and so their parental bodies. Even if those analogues can be suitable guideline they cannot take into account the spectral variability of the investigated samples and bodies.

Because to implement suitable systematic mixture of mineral powders with similar composition to those present for example into the HED is not an easy task to pursue, so to take advantage of the heterogeneity of natural sample could be an useful tool to enlarge the knowledge about spectral trends for these materials.

## 5. Conclusions

NWA6232 is an olivine diogenite characterized by an average 25% of olivine, with an heterogeneous texture. Olivine is present in euhedral and subhedral crystals from μm to mm in scale, often poikilitically included in orthopyroxene crystals. Clast of mm sizes of olivine and orthopyroxene were also present. This heterogeneity have been considered to investigate the VNIR reflectance variability from the slab surfaces of two different slices.

In general, the reflectance of the ol-diogenite is characterized by the two absorptions around 1 and 2 μm due to the presence of the orthopyroxene. The orthopyroxene rich area spot and the powder samples prepared from a representative portion of one slice show absorption on the same positions but with different intensity. The band center positions are close to those of synthetic pyroxene with similar composition from Klima et al. (2007), even if shifted at higher wavelengths, in accordance with the presence of widespread olivine in NWA6232.

Then we used the presence of a rounded ol-clast of circa 6mm size in diameter to evaluate also the spectral variability varying the ol abundance within the measured spot. The spectra acquired in the ol-clast show clearly the wide absorption band at ~1 μm typical of olivine, moreover a residual absorption at at ~2 μm is still present due to the presence of chromites crystal within the ol-clast. The position of the olivine absorption is in accordance with those from the literature with similar composition (e.g. Isaacson et al. 2014).

Spectral parameters like B.A.R and B.S. showed that a shift towards the values attributable to the ol-clast is already reached for 30% of the clast into the spot.

Conversely, we have seen that the B.C.I position is in accordance with the trend present in Pieters et al. (2005) evidenced for ol-px mineral mixtures, once compare with B.A.R values. In addition, B.C.I position shows a linear trend from the synthetic orthopyroxene to olivine clast with respect to the olivine areal %, suggesting a 8% of olivine present into the ol-diogenite. This value is underestimated from the 20-35% range measured by SEM image analysis for different images acquired from the samples. This results indicate how

pyroxenes absorption dominates the spectra until ~30% of the olivine abundance, for En-Wo and Fa composition suitable for diogenites.

Those results evidence the importance to work on slab spectra. The spectral variability of HED slices should be considered to enlarge the number of studied samples and to use the heterogeneity of those meteorites to investigate much more in details spectral parameters trends and property, considering minerals composition suitable to the different diogenites and eucrites.

## 6. References


Ammannito E. , De Sanctis M. C. , Capaccioni F. , et al. 2013a. Vestan lithologies mapped by the Visual and InfraRed spectrometer on Dawn. Meteoritics and Planetary Science 48: 2185–2198.

Ammannito E., De Sanctis M. C. , Palomba E., et al. 2013b. Olivine from Vesta's mantle exposed on the surface. Nature 504: 122–125.

Beck A. W. and McSween H. Y. 2010. Diogenites as polymict breccias composed of orthopyroxenite and harzburgite. Meteoritics and Planetary Science 45: 850–872.

Beck A. W., McCoy T. J. , Sunshine J. M. et al. 2013. Challenges in detecting olivine on the surface of 4 Vesta. Meteoritics and Planetary Science 48: 2155–2165.

Beck P., Barrat J.-A., Frisolle F., Quirico E., Schmitt B., Moynier F. Gillet P., Beck C. 2011. NIR spectral trends of HED meteorites: Can we discriminate between the magmatic evolution, mechanical mixing and observation geometry effects? Icarus 216, 560–571.

Burbine T. H., Buchanan P. C., Dolkar T., et al. 2009. Pyroxene mineralogies of near-Earth Vestoids. Meteoritics and Planetary Science 4: 1331–1341.

Burns R. 1993. Mineralogical Applications of Crystal Field Theory, 2nd ed. Cambridge University Press. 551 p.

Carli C. and Sgavetti M. 2011. Spectral characteristics of rocks: Effects of composition and texture and implications for the interpretation of planet surface compositions. Icarus 211: 1034–1048.

Carli C., Ciarniello M., Capaccioni F. Serventi G. and Sgavetti M. 2014a. Spectral variability of plagioclase–mafic mixtures (2): Investigation of the optical constant and retrieved mineral abundance dependence on particle size distribution. Icarus 235: 207–219. doi:10.1016/j.icarus.2014.03.022.

Carli C., Serventi G. and Sgavetti M., 2014b. VNIR spectral variability of the igneous stratified Stillwater Complex: A tool to map lunar highlands. American Mineralogist 99: 1834–1848. doi: 10.2138/am-2014-4808.

Carli C., Serventi G. and Sgavetti M., 2015. VNIR spectral characteristics of terrestrial igneous effusive rocks: Mineralogical composition and the influence of texture. In: Platz, T., Massironi, M., Byrne, P.K., Hiesinger, H. (Eds.), Volcanism and Tectonism Across the Inner Solar System, vol. 401. Geological Society, London, Special Publications, pp. 139–158, doi: 10.1144/SP401.19 (first published online June 17, 2014).

Clark R. N. and Roush T. L. 1984. Reflectance spectroscopy: Quantitative analysis techniques for remote sensing applications. Journal of Geophysical Research 89: 6329–6340.

Cloutis E. A., Gaffey M. J., Jackowski T. L. et al. 1986. Calibrations of phase abundance, composition, and particle size distribution for olivine-orthopyroxene mixtures from reflectance spectra. Journal of Geophysical Research 91: 641–653 .

Cloutis E. A., Sunshine J. M. and Morris R. V. 2004. Spectral reflectance-compositional properties of spinels and chromites: Implications for planetary remote sensing and geothermometry. Meteoritics and Planetary Science 39, 545–565.

Cloutis E. A. and Gaffey M. J. 1991. Pyroxene spectroscopy revisited: spectral-compositional combinations and relationships to geothermometry. Journal of Geophysical Research 96: 22809–22826.

Craig, M. A., Cloutis, E. A., Reddy, V., Bailey, D. T. and Gaffey, M. J. 2007. The Effects of Grain Size, <45–1000 μm, on the Reflectance Spectrum of Planetary Analogs from 0.35–2.5 μm. 38th Conference on Lunar Planetary Science, Abstract 1356.

Craig, M. A., Cloutis, E. A., Reddy, V., Bailey, D. T. and Gaffey, M. J. 2008. The Effects of Grain Size, <10 μm – 4.75 mm, on the Reflectance Spectrum of Planetary Analogs from 0.35–2.5 μm. 39th Conference on Lunar Planetary Science, Abstract 2082.

De Sanctis M.C. et al. (2010) The VIR Spectrometer. In: Russell C., Raymond C. (eds) The Dawn Mission to Minor Planets 4 Vesta and 1 Ceres. Springer, New York, NY.

Duffard R. Lazzaro D. and DeLeon J. 2005. Revisiting spectral parameters of silicate-bearing meteorites. Meteoritics & Planetary Science 40, Nr 3, 445–459

Freierberg M.A. and Drake M.J. 1980. The Meteorite-Asteroid Connection: The Infrared Spectra of Eucrites, Shergottites, and Vesta. Science, 209, 805-807. DOI: 10.1126/science.209.4458.805.

Gaffey, M. J., Bell J. F. and Brown R. H. et al. 1993. Mineralogical variations within the S-type asteroid class. Icarus 106, 573–602.

Garvie L. A. J. 2012. The Meteoritical Bulletin, No. 99, April 2012. doi/10.1111/maps.12026

Grady M. M., Pratesi G., Moggi Cecchi V. 2015. Atlas of Meteorites. 1st Ed. Cambridge University Press. p 384.

Isaacson P. J., Klima R. L., Sunshine J. M., Cheek L. C., Pieters C. M., Hiroi T., Dyar M. D., Lane M. and Bishop J. 2014. Visible to near-infrared optical properties of pure synthetic olivine across the olivine solid solution. American Mineralogist, 99, 467-478. Doi:10.2138/am.2014.4580.

Harloff, J. and Arnold, G. 2001. Near-infrared reflectance spectroscopy of bulk analogue materials for planetary crust. Planetary Space Science, 49, 191–211.

Hiroi T., Pieters C. M., Vilas F., Sasaki S., Hamabe Y., and Kurahashi E. 2001. The mystery of 506.5 nm feature of reflectance spectra of Vesta and Vestoids: Evidence for space weathering? Earth Planets Space, 53, 1071–1075,

King, T.V.V. and W.I. Ridley 1987. Relation of the Spectroscopic Reflectance of Olivine to Mineral Chemistry and Some Remote Sensing Implications, J. Geophys. Res. 92, 11457-11469

Klima, R. L., Pieters, C.M. & Dyar, M. D. 2007. Spectroscopy of synthetic Mg-Fe pyroxenes I: spinallowed and spin-forbidden crystal field bands in the visible and near-infrared. Meteoritics & Planetary Science, 42, 235–253.

Li S. and Milliken R.E. 2015 Estimating the modal mineralogy of eucrite and diogenite meteorites using visible–near infrared reflectance spectroscopy. Meteoritics & Planetary Science 1–30 (2015). Doi: 10.1111/maps.12513

McSween H. Y., Binzel R. P., De Sanctis M. C. et al. 2013. Dawn; the Vesta–HED connection; and the geologic context for eucrites, diogenites, and howardites. Meteoritics & Planetary Science 48, 2090-2104. Doi: 10.1111/maps.12108.

Mittlefehldt, D.W. , McCoy, T.J. , Goodrich, C.A. , et al. , 1998. Non-chondritic meteorites from asteroids bodies. In: Papike, J.J. (Ed.). Planetary Materials, Chapter 4, Mineralogical Society of America, vol. 36 .

Moskovitz N. A., Willman M., Burbine T. H., Binzel R. P., Bus S. J. 2010. A spectroscopic comparison of HED meteorites and V-Type asteroids in the inner Main Belt. Icarus, 208, 773-788

Palomba E. , Longobardo A. , De Sanctis M. C. , et al. , 2015. Detection of new olivine-rich locations on Vesta. Icarus 258, 120–134 .

Peslier A.H., Brandon A.D., Tarduno J.A. and Mittlefehldt D.W. (2015) Petrology of diogenite NWA 5480, a pristine olivine-riche deformed harzburgite. 46th Lunar and Planetary Science Conference, abs. 2221.

Pieters C. M., Binzel R. P., Bogard D., Hiroi T., Mittlefehldt D. W., Nyquist L., Rivkin A., and Takeda H. 2005. Asteroid-meteorite links: The Vesta conundrum(s). Proceedings of the International Astronomical Union 1:273–288.

Pompilio, L., Sgavetti, M.&Pedrazzi, G. 2007. Visible and near-infrared reflectance spectroscopy of pyroxene-bearing rocks: new constraints for understanding planetary surface compositions. Journal of Geophysical Research, 112, E01004, http://dx.doi.org/10.1029/2006JE002737.

Poulet F. , Ruesch O. , Langevin Y. , et al. ,2015. Modal mineralogy of the surface of Vesta: Evidence for ubiquitous olivine and identification of meteorite analogue. Icarus 253, 354–377.

Ruesch O. , Hiesinger H. , De Sanctis M. C. et al. 2014. Detections and geologic con-text of local enrichments in olivine on Vesta with VIR/Dawn data. Journal of Geophysical Research 119, 2078–2108.

Serventi G. and Carli C. 2017. The role of very fine particle sizes in the reflectance spectroscopy of plagioclase-bearing mixtures: New understanding for the interpretation of the finest sizes of the lunar regolith. Icarus 293, 157-171.

Serventi G., Carli C., Sgavetti M., 2016. Deconvolution of mixtures with high plagioclase content for the remote interpretation of lunar plagioclase-rich regions. Icarus, 272, 1-15. Doi: 10.1016/j.icarus.2016.01.020.

Serventi G. , Carli C. , Sgavetti M., Ciarniello M., Capaccioni F. 2013. Spectral variability of plagioclase–mafic mixtures (1): Effects of chemistry and modal abundance in reflectance spectra of rocks and mineral mixtures. Icarus 226, 282–298 .

Sunshine J. M., Pieters C. M., Pratt S. F. 1990. Deconvolution of mineral absorption bands: An improved approach. Journal of Geophysical Research 95, 6955–6966.

Sunshine J. M., Pieters C. M., 1998. Determining the composition of olivine from reflectance spectroscopy. J. Geophys. Res. 103, 13675–13688.

Thangjam G., Nathues A., Mengel K., Hoffmann M., Scheafer M., Reddy V., Cloutis E. A., Christensen U., Sierks H., Le Corre L., Vincent J-B., and Russell C. T. 2014. Olivine-rich exposures at Bellicia and Arruntia craters on (4) Vesta from Dawn FC. Meteoritics & Planetary Science 49, 1831–1850.

Tkalcec B.J., Golabek G.J. and Brenker F.E. (2013)

Solid-state plastic deformation in the dynamic interior of a differentiated asteroid. Nature Geoscience, 6, 93-97.
Zambon F., De Sanctis M. C. , Schröder S. E. , et al., 2014. Spectral analysis of the bright materials on the Asteroid Vesta. Icarus 240, 73–85.
Zambon F., Tosi F., Carli C., et al. 2016. Lithologic variation within bright material on Vesta revealed by linear spectral unmixing. Icarus, 272, 16-31. Doi: 10.1016/j.icarus.2016.01.009.
Yamaguchi A., Barrat J.A., Shirai N., and Ebihara M. (2015) Petrology and geochemistry of Northwest Africa 5480 diogenite and evidence for a basin-forming event on Vesta. Meteoritics & Planetary Science 50, 1260–1270.

## 7. Figure Captions

Figure 1 – It shows the two slab samples a) NWA6232_A and b) NWA6232_B. Powders and a thin section have been produced from NWA6232_B representative of the ol diogenite. In a) is shown the ol clast with a green circle whereas in b an arrow indicates a portion of opx enriched portion. C) Polarizing optical microscope image of thin section: grey crystals are orthopyroxene; pink to blue crystals are olivine; the outlined area is poikilitic olivine in an orthopyroxene crystal; transmitted light, crossed polars.

Figure 2 – Selected spectra of slabs, a-d), and powders at variable grain size are plotted in e). a) ol-clast spectra (NWA6232_A), b) spectra characterized by ol-richer portions, c) ol-diogenite spectra, d) spectra relatedto the opx rich portion of NWA6232_B. e)from bottom to top <50, <75, <100, <125, <150, <180, <200, <250 μm.

Figure 3 – Spin-forbidden in the visible spectral range. a) selected spectra from different spot, green spectra are related to higher abundance of olivine, violet spectra indicate ol-diogenite o px-rich portion. b) continuum removed spectra to highlight the differences, powder continuum removed spectra are reported as comparison.

Figure 4 – ol-cross section and spectra. In a) is showed the portion from which we moved out to in the ol-clast. In b) all spectra are showed (see table 3) and in c) continuum removed spectra of the first, last and one intermediate spectra.

Figure 5 – a,b) averaged Band Centers are related to the Fs% of diogenite opx, with the band center of the closest synthetic opx from Klima et al. (2007) for a comparison. c) Band I center is plotted versus Band II center, average values for the two slabs, powders and synthetic opx are present as well as outliers ol-rich and ol-clast position. Green line represent the position of B.C.I for ol with similar composition, dashed: King and Ridley et al. 1987, solid: Sunshine and Pieters 1998, and dot: Isaacson et al., 2014. Error band are the standard deviation of the average.

Figure 6 – Band depth I, II (a,b) and Band Shoulder (c,d) are plotted vs the Band Center I, II. Band Center I of ol-cross spectra has been plotted vs. the B.A.R, moreover we have plotted the averaged values for powders, which is very close to the ol-diogenite (000, 001) spectra. See text for more details.

Figure 7 – Ol-clast abundance within the spot has been compare with the Band Center I (a) and B.A.R (b). Band Center shows a linear relationship. c) Band I center has been plotted in function of the ol abundance, taking into account the synthetic px has free-ol endmember. The trend see in a), related to green square shift towards higher abundance of ol (green diamonds, in fact spot 000 is not anymore 0% of ol). Considering that the best linear fit should be obtain for an 8% of widespread ol into the diogenite, but SEM

images analysis reveal an higher value, ~25%. We plot also the averaged values for powders (orange cross) and ol-diogenite slabs (blu triangle). See text for more details.

**Figure:**


**Figure 1**

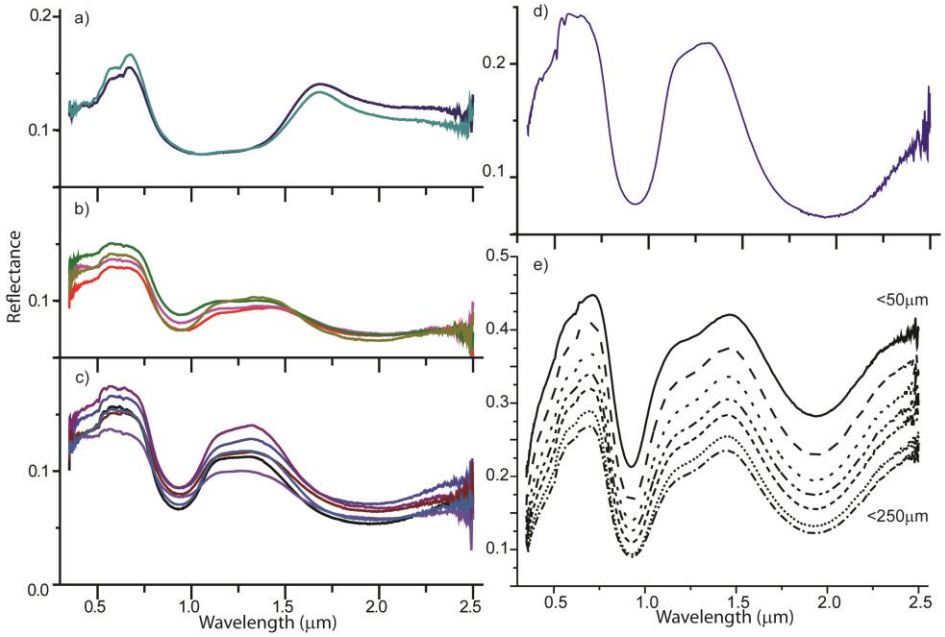


**Figure 2**

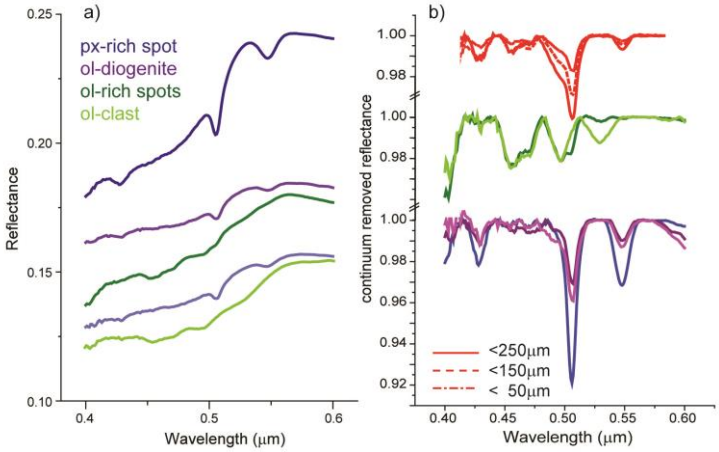


**Figure 3**

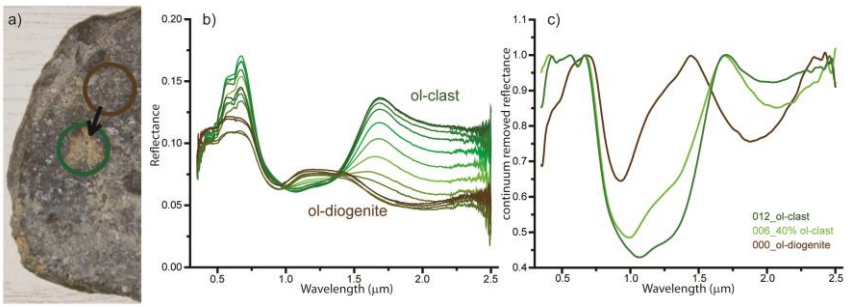


**Figure 4**

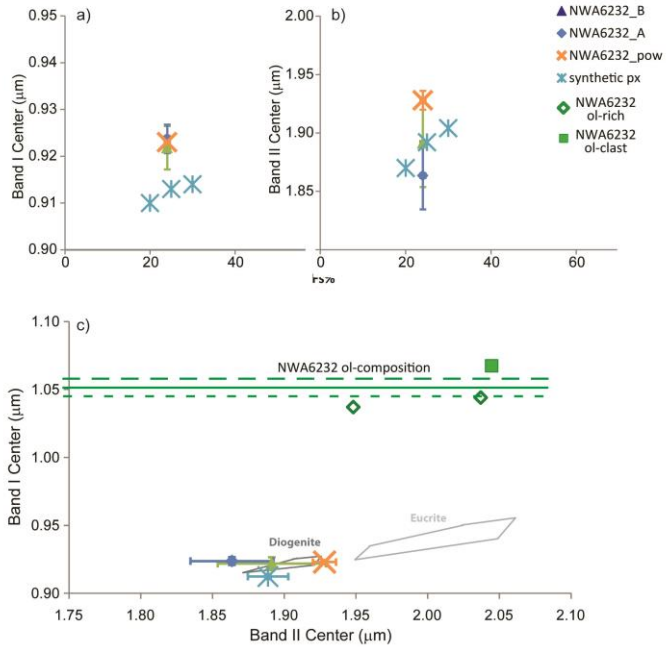


**Figure 5**

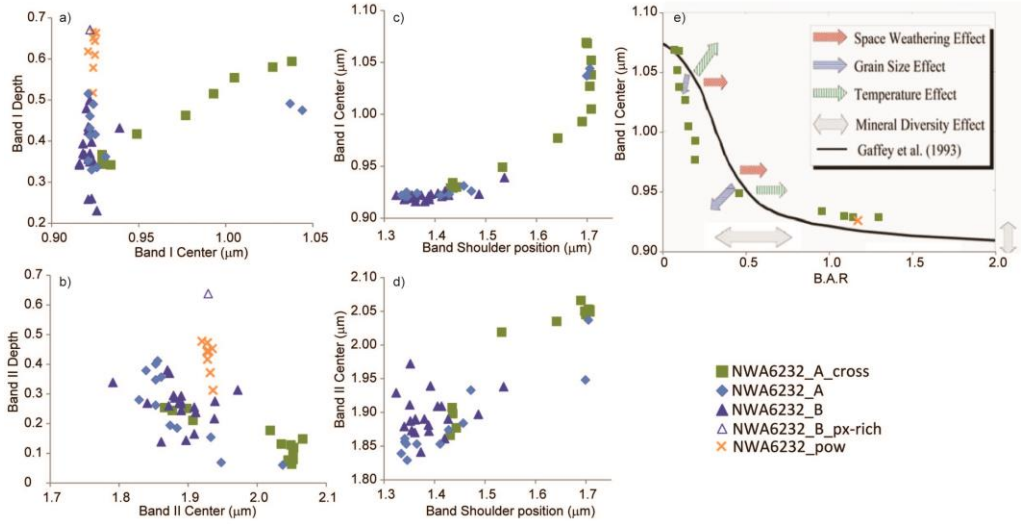


**Figure 6**

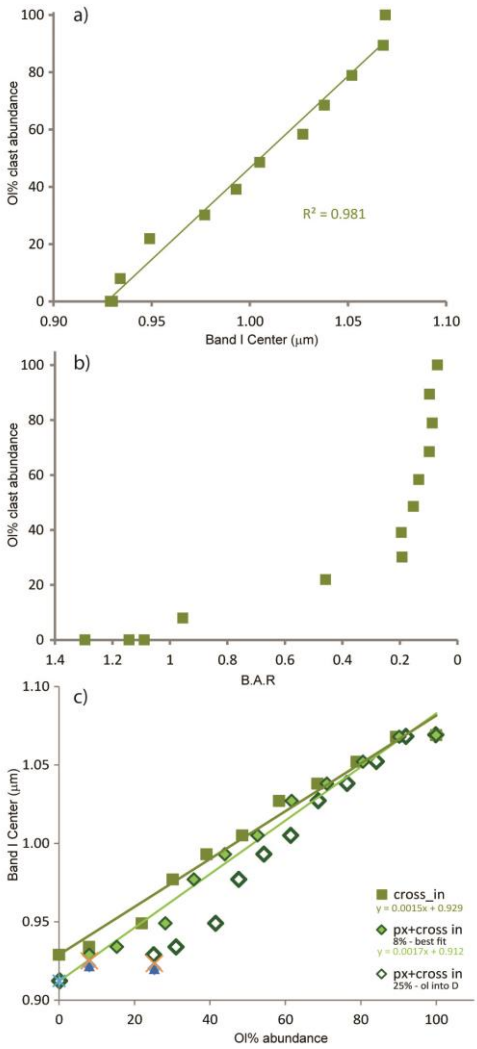


**Figure 7**

Tables:

Table 1. relative abundance retrieved from SEM image analysis. See text for more details.

| | modal distribution ol-diogenite | | | | | | modal distribution ol-clast | | | | |
|---|---|---|---|---|---|---|---|---|---|---|---|
| | mean | st.dev | spot 1 | spot 2 | spot 3 | spot 4 | mean | st.dev | spot 5 | spot 3 | spot 4 |
| **Olivine** | **25.7** | 6.1 | 34.5 | 22.4 | 25.0 | 20.8 | **96.5** | 1.9 | 98.6 | 94.8 | 96.0 |
| **Pyroxene** | **71.8** | 5.6 | 63.7 | 72.6 | 74.3 | 76.5 | rare | | | | |
| **Chromite** | **0.9** | 0.3 | 1.1 | 1.1 | 0.5 | 0.8 | **2.9** | 1.7 | 0.8 | 3.8 | 3.9 |
| **Troilite** | **1.2** | 0.9 | 0.7 | 1.9 | 0.3 | 2.0 | **0.7** | 0.7 | 0.5 | 1.4 | 0.1 |
| **Fe,Ni alloy** | rare | | | | | | rare | | | | |

Table 2. Mineral chemistry for the major phase as retrieved from microprobe analysis

| | pyroxene | | | olivine | |
|---|---|---|---|---|---|
| | mean | st.dev. | | mean | st.dev. |
| **SiO2** | 54.7 | 0.6 | **SiO2** | 37.4 | 0.5 |
| **TiO2** | 0.1 | 0.1 | **TiO2** | 0.0 | 0.1 |
| **Al2O3** | 0.4 | 0.0 | **Al2O3** | 0.0 | 0.0 |
| **Cr2O3** | 0.5 | 0.2 | **Cr2O3** | 0.1 | 0.1 |
| **FeO** | 15.7 | 0.5 | **FeO** | 26.2 | 0.8 |
| **Mno** | 0.5 | 0.1 | **Mno** | 0.6 | 0.1 |
| **MgO** | 27.1 | 0.3 | **MgO** | 35.8 | 0.5 |
| **CaO** | 1.0 | 0.1 | **CaO** | 0.1 | 0.1 |
| **Na2O** | 0.0 | 0.0 | **Na2O** | 0.0 | 0.1 |
| **K2O** | 0.0 | 0.1 | | | |
| **Total** | 100.1 | 0.7 | **Total** | 100.2 | 0.8 |
| | | | | | |
| **Wo** | 2.0 | 0.2 | **Fo%** | 70.5 | 0.9 |
| **En** | 73.8 | 0.8 | **Fa%** | 29.5 | 0.9 |
| **Fs** | 24.1 | 0.6 | | | |
| **N° Mg** | 75.4 | 0.7 | **N° Mg** | 70.9 | 0.9 |

711

Table 3. Steps from out to in the clast of olivine in NWA6232_A, and relative % of olivine clast into the spot

| | Ol cross | |
|---|---|---|
| spot | step (mm) | Area ol clast% |
| 000 | 8.0 | 0.0 |
| 001 | 7.0 | 0.0 |
| 002 | 6.0 | 0.0 |
| 003 | 5.0 | 7.9 |
| 004 | 4.0 | 21.9 |
| 005 | 3.5 | 30.2 |
| 006 | 3.0 | 39.1 |
| 007 | 2.5 | 48.5 |
| 008 | 2.0 | 58.3 |
| 009 | 1.5 | 68.5 |
| 010 | 1.0 | 78.9 |
| 011 | 0.5 | 89.4 |
| 012 | 0.0 | 100.0 |

712